Integrating Micropower Impulse Radar and Motes[1]

Prabal K. Dutta

Department of Electrical Engineering, The Ohio State University
205 Dreese Laboratories, 2015 Neil Ave, Columbus, Ohio 43210
`dutta.4@osu.edu`

Abstract. Distributed wireless sensor networks hold great promise as an enabling technology for a variety of applications. Distributed target tracking is one such envisioned application for sensor networks. In this paper, we develop a ranging and tracking model using commercially available micropower impulse radars integrated with small computing and communicating devices called "motes."

1   Introduction

Micropower impulse radar (MIR) is a promising technology that was developed in the mid 1990s at Lawrence Livermore National Labs. The technology enables credit card-sized radar detectors that can be used for a wide variety of purposes including motion detection and velocity estimation. By integrating MIR with small devices called "motes" that capable of computing and wirelessly communicating, we can build distributed networks of sensors that can detect and track a variety of targets and provide rich situational awareness for use in commercial and defense applications. In this paper, we investigate the Advantaca MIR sensor, develop interfacing hardware, write test software, and develop algorithms for single-sensor target ranging, multi-sensor target localization and distributed tracking.

2   Micropower Impulse Radar Sensor

We use the TWR-ISM-002 sensor from Advantaca [l] as our MIR platform. This sensor detects *motion* up to a 60ft radius around the sensor but this range is adjustable to a shorter distance using an onboard potentiometer. The unit's sensitivity can also be adjusted in a similar fashion, depending on environmental considerations like proximity to the ground and presence of clutter. Multiple MIR sensors can be co-located and simultaneously operate without interference due to the pseudorandom nature of the MIR transmissions.

The sensor includes a 51-pin connector designed to interface mechanically with the expansion connector on the Mica Motes [2]. The MIR provides a digital output via pin 25 of the connector indicating the presence (low) or absence (high) of a *moving* target within the sensor's range. This output is a fast-attack

and slow-decay meaning that the output is asserted immediately after detecting a target but is not unasserted until approximately one second after the target is no longer detected. A *stationary* target is not detected with this particular MIR sensor. The MIR also provides an analog output accessible via pin 42 on the 51-pin connector. The analog signal varies from 0V to 2.5V and is nominally centered at 1.25V when there is no motion (*i.e.* the quiescent state). The analog output varies between 0V - 2.5V when there is motion toward or away from the MIR. The output signal is a clipped sinusoid at the Doppler frequency and is proportional to the component of the target's velocity in the direction toward or away from the MIR. The clipped sinusoidal output signal encounters a zero crossing (or 1.25V bias, in this case) for every $l/2$ units of distance the target travels. The MIR sensor's operating frequency f = 2.4GHz, giving us a wavelength l = c / f = 3.0×10^8 / 2.4×10^9 = 12.5 cm. Therefore, the analog output crosses zero for every $l/2$ = 6.25 cm of travel toward or away from the sensor. The analog output returns to 1.25V when motion stops. The elapsed time t_z between successive zero crossings is inversely proportional to the target's radial velocity (the target's velocity along the sensor's line of sight) with a proportionality constant of $l/2$. Therefore, the radial velocity $v_r = l/2t_z$.

Despite the mechanical compatibility through the expansion connector interface, matching signal pin assignments, and common power pin assignments, the MIR and Mica motes require *different* and *incompatible* operating voltages. The Mica motes require, and through the expansion connector provide, the raw battery voltage that can vary from 3.0V nominally to 2.7V or lower.

The MIR unit requires 3.4V – 6.0V (nominally 3.6V) drawing less than 1mA on pin 50 of the expansion connector. The unit also requires a precise power source to provide 5.5V with a ±1% tolerance drawing a nominal 7.5mA on pin 2 of the expansion connector. Finally, the MIR requires PW4 (pin 33) to be asserted high in order to run.

3 Mica Power Board

Since the voltages required by the MIR exceed the voltages provided by the Mica, we designed a circuit consisting of a pair of boost switching regulators to generate these higher voltages. The Mica Power Board implements this circuit and is shown in Figure 1. A schematic of the switching regulator is shown in Figure 2. The board owes its odd footprint with a U-shaped cutout in the upper left and a square with rounded corners in the middle to a desire to maintain physical compatibility with the existing Mica Sensor Board.

The Mica Power Board has two fully independent switching regulators that are potentiometer adjustable, via R2 and R5, and can deliver 3V – 40V at 200 mA each through signals VDD1 and VDD2, respectively, via pins 2 and 50 on the *top* expansion connector. The circuit works by intercepting the two power signals available through the *bottom* expansion connector and replacing these

signals with the outputs of the two regulators and then passing the regulator output through the *top* connector.

The Mica Power Board also includes a power down (SHUTDOWN) feature. Asserting PW0 (pin 29) and PW1 (pin 30) will enable (turn on) the regulator VDD1 and VDD2, respectively. If one or both of these pins are not asserted, then the regulator is in a passive mode that allows Vcc to pass through the regulator so that VDD1 = Vcc and/or VDD2 = Vcc. If neither PW0 nor PW1 is asserted, then the regulator appears electrically "invisible."

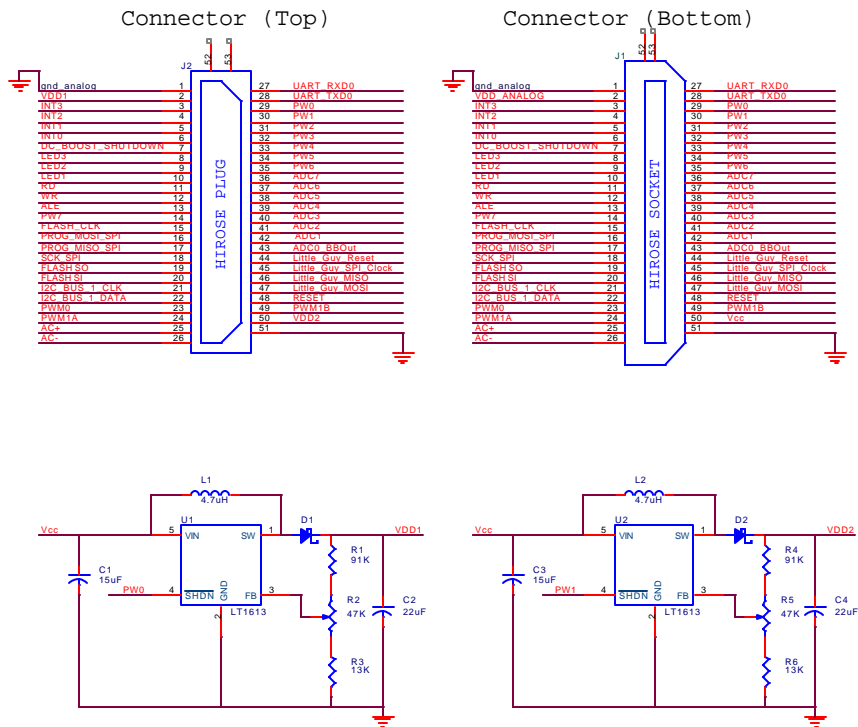**Figure 1: The Mica Power Board.**

Figure 2: Mica Power Board Schematic

When used with the MIR board, **VDD1 must be set to 5.5V and VDD2 must be set to 3.6V. Failing to do so will destroy the MIR units.** VDD1, VDD2, and GND are all available through test points in the upper left, upper middle, and upper right parts, respectively, of the Mica Power Board. **We strongly recommend that the presence of these voltages be confirmed prior to attaching the MIR sensor**. If the specified voltages do not appear at the test vias, adjust R2 and R5 until these voltages appear. Placing a small dot of nail polish on R2 and R5 after these adjustments helps ensure the potentiometer settings are not changed accidentally. *Note that there must a software driver that asserts* PW0 *and* PW1 *running on an attached Mica2 mote (see the section on software).*

4 Mechanical Configuration

The Mica mote, Mica Sensor Board, Mica Power Board, and MIR board should be stacked as shown in Figure 3. **Stacking the circuit boards in any other configuration will destroy the electronics**, so caution should be used. Note, however, that the presence of the Mica Sensor Board is optional and no harm will be done if it is not present.
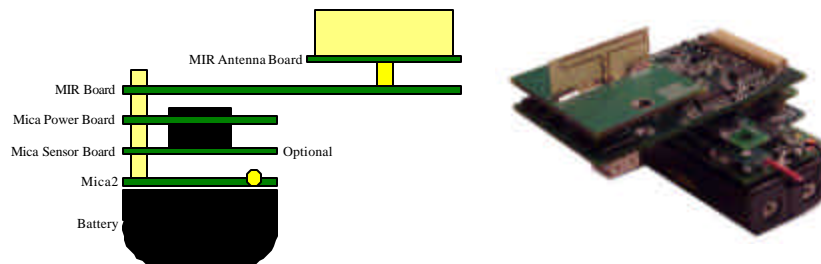

Figure 3: Stacking configuration of circuit boards.

5 Software

We provide a simple test program written in nesC/TinyOS to verify proper operation of the Mica Sensor Board and MIR board. This test program does not qualify as a "real" driver in that it is not written to interoperate with other programs. Its purpose is to demonstrate operation of the Mica Power Board and the MIR sensor.

`PowerRead.nc` – Configuration file.
`PowerReadM.nc` – Implements test driver.
`ReadData.nc` – Provides an interface to read data.

Listing 1: Program to verify operation of MIR and Mica Power Board.

6　Ranging

The MIR sensors available to us were *motion* sensors and not *rangefinders*. However, it is possible to use the analog output of the sensor to determine the target's range, as discussed in this section. Our model assumes the following:

1. The MIR sensor's field of view is a hemisphere whose projection onto the *x-y* plane is a circle of radius *r* with the sensor located at the center point O. The area enclosed by the circle is the sensitive area of the sensor and sometimes we call this area the *detection circle* or *detection zone*. The maximum *detection range* of the sensor is equal to the radius *r* of the circle.
2. The target's trajectory passes through a secant or diameter of the detection circle. If the target's trajectory is a tangent or non-intersecting line, the sensor does not detect the target's passage.
3. A *single* target at a time moves through the sensor's field of view at a relatively constant speed v_0 and with an arbitrary but constant heading. We can tolerate small variations in speed, as long the target's speed remains above a certain lower bound. An implication of the prior requirement is that the target does not reverse direction. Violating these assumptions leads to poor range estimation at best and completely useless range estimation at worst.
4. The initial detection time t_0 corresponds to the target's entry point into the detection circle and the final detection time t_1 and corresponds to the target's exit from the detection zone.

Figure 4 depicts the above assumptions geometrically. We will refer to this model during our derivation of the range estimation equations.
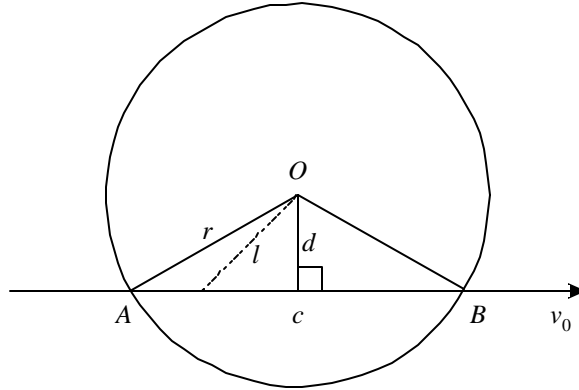

Figure 4: Ranging model.

Even though the MIR does not directly provide a range measure to the target, it is possible to compute this information from the analog output of the MIR sensor. Let *c* be the length of the chord AB traversed by the target and let *d* be

the shortest distance from the center of the detection circle O to the chord AB. The chord length $c = 2 \times (r^2 - d^2)^{1/2}$. At the point where the target first enters the detection circle, the target's range l from the sensor is equal to the detection radius r. At the closest point of approach, or CPA, the target's range from the sensor is d. And, at the point of exit from sensor's field of view, the target's range is once again r.

We can determine d by recognizing that the target travels a distance of $r - d$ in the radial direction toward the center of the circle and then an equal distance away from the center, giving a total radial distance traversed of $2(r - d)$. Recall that the analog output produces a zero crossing for every $l/2$ units of distance the target travels in the radial direction. If we let k be the number of zero crossings counted during the interval from t_0 to t_1, then $2(r - d) = kl/2$. Rearranging we have $d = r - kl/4$. Since r and l are constant, and k is countable with very little signal processing (*i.e.* simple zero crossing detection), d is easily computable *ex post facto*.

Now, let us compute the target's range as a function of time. We begin by determining the target's progression along the chord c_p as function of time. Since the target travels with velocity v_0 and enters the circle at time t_0, the progression of the target along c is given by $c_p(t) = v_0 \cdot (t - t_0)$; $\forall t \mid t_0 \le t \le t_1$. To simplify our derivation, assume that the sensor is located at $O = (0, 0)$. Then, we can write the target's position along the x-axis as $x(t) = v_0 \cdot (t - t_0) - (r^2 - d^2)^{1/2}$; $\forall t \mid t_0 \le t \le t_1$. This function's range is $[-c/2, c/2]$.

Let q denote the angle enclosed by l and d. We can easily compute q as a function of time, giving $q(t) = \text{Tan}^{-1} (|x(t)|/d)$; $d \ne 0$. In the interest of symmetry and a cleaner derivation, we rewrite this equation to let $q(t)$ be an odd function whose range is $(-\pi/2, \pi/2)$: $q(t) = \text{Tan}^{-1} (x(t)/d)$.

It should be clear that $\forall t \mid t_0 \le t \le t_1$

$$l(t) = d/\cos q(t)$$

where

$$d = r - kl/4$$
$$q(t) = \text{Tan}^{-1} (x(t)/d)$$
$$x(t) = v_0 \cdot (t - t_0) - c/2$$
$$c = 2 \cdot (r^2 - d^2)^{1/2}$$
$$v_0 = c/(t_1 - t_0)$$

Combining these equations into a function consisting of only the variables t, t_0, t_1, k, r, and l yields

$$range(t, t_0, t_1, k, r, \boldsymbol{l}) = \frac{r - \dfrac{k\boldsymbol{l}}{4}}{\cos\left(\tan^{-1}\left(\dfrac{2 \times \sqrt{r^2 + \left(r - \dfrac{k\boldsymbol{l}}{4}\right)^2 \left(\dfrac{t - t_0}{t_1 - t_0} - \dfrac{1}{2}\right)}}{r - \dfrac{k\boldsymbol{l}}{4}}\right)\right)}$$

which, due to the presence of cosine, arctangent, and square roots is not efficient from a computation point of view. A nearly linear approximation can be used with reasonable results. For example, the following approximation

$$\text{range\_approx}(t, t0, t1, k, r, \lambda) := \frac{k \cdot \lambda}{4} \cdot \left(\left|1 - \left|\frac{2 \cdot t}{t1 - t0} - 1\right|\right|\right) + r$$

provides reasonably low error in certain cases. We leave it to the reader to determine the worst-case performance and fitness for use.
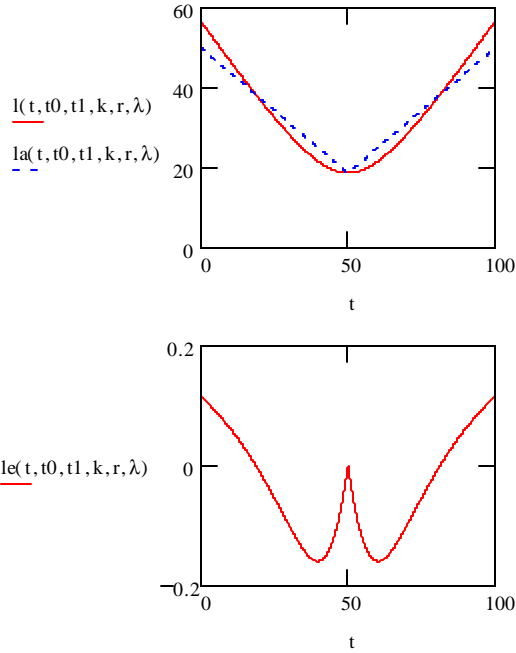

Figure 5: (a) range (solid line), approximation (dotted line); (b) error.

We again emphasize that this approach is predicated on the assumption that a *single* target moves through the sensor's field of view at a relatively constant speed v_0 and with an arbitrary but constant heading.

7   Conclusion

We demonstrated the integration of a micropower impulse radar sensor with the Mica2 motes and developed algorithms for ranging. In the future, we will extend our work to include localization and tracking of single and multiple targets as well as targets whose speeds change.

[1] http://www.advantaca.com
[2] http://webs.cs.berkeley.edu/tos/hardware/hardware.html